Terpene emissions from boreal wetlands can initiate stronger atmospheric new particle formation than boreal forests

Junninen, Heikki

2022-04-19

ARTICLE

Check for updates

Terpene emissions from boreal wetlands can initiate stronger atmospheric new particle formation than boreal forests

Heikki Junninen [1,2✉], Lauri Ahonen [1], Federico Bianchi [1], Lauriane Quéléver[1], Simon Schallhart[1,3], Lubna Dada [1], Hanna Elina Manninen[1], Katri Leino[1], Janne Lampilahti[1], Stephany Buenrostro Mazon [1], Pekka Rantala [1], Mari Räty [1], Jenni Kontkanen [1], Sara Negri[4], Diego Aliaga[1], Olga Garmash [1], Pavel Alekseychik[1,5], Helina Lipp[2], Kalju Tamme[2], Janne Levula[1], Mikko Sipilä[1], Mikael Ehn [1], Douglas Worsnop[1], Sergej Zilitinkevich [1,3], Ivan Mammarella [1], Janne Rinne [6], Timo Vesala[1], Tuukka Petäjä [1], Veli-Matti Kerminen[1] & Markku Kulmala [1✉]

Aerosols and their interaction with clouds constitute the largest uncertainty in estimating the radiative forcing affecting the climate system. Secondary aerosol formation is responsible for a large fraction of the cloud condensation nuclei in the global atmosphere. Wetlands are important to the budgets of methane and carbon dioxide, but the potential role of wetlands in aerosol formation has not been investigated. Here we use direct atmospheric sampling at the Siikaneva wetland in Finland to investigate the emission of methane and volatile organic compounds, and subsequently formed atmospheric clusters and aerosols. We find that terpenes initiate stronger atmospheric new particle formation than is typically observed over boreal forests and that, in addition to large emissions of methane which cause a warming effect, wetlands also have a cooling effect through emissions of these terpenes. We suggest that new wetlands produced by melting permafrost need to be taken into consideration as sources of secondary aerosol particles when estimating the role of increasing wetland extent in future climate change.

[1] Institute for Atmospheric and Earth System Research INAR / Physics, University of Helsinki, Helsinki, Finland. [2] Institute of Physics, University of Tartu, Tartu, Estonia. [3] Finnish Meteorological Institute, Helsinki, Finland. [4] Department of Agricultural, Forest and Food Sciences, University of Turin, Turin, Italy. [5] Bioeconomy and Environment, Natural Resources Institute Finland (LUKE), Helsinki, Finland. [6] Department of Physical Geography and Ecosystem Science, Lund University, Lund, Sweden. ✉email: heikki.junninen@ut.ee; markku.kulmala@helsinki.fi

Wetlands are important when assessing the climatic influence of land cover because of their multifold role in climate forcing. As discussed below in more detail, wetlands emit methane (CH_4) and volatile organic compounds (VOCs), such as isoprene and monoterpenes, and represent an important sink for atmospheric carbon dioxide (CO_2). Through the atmospheric oxidation of VOCs and following gas-to-particle conversion, wetlands are also source of secondary organic aerosols. However, virtually no studies exist on aerosol formation from wetland emissions[1]. CH_4 is the second most important greenhouse gas after CO_2. Approximately, 40% of CH_4 emissions are from natural sources, mainly wetlands[2]. Northern peatlands[3] (i.e., latitude 40°–70°N) emit about 36 Tg CH_4-C per year[4,5], which is equivalent to 11% of the total CH_4 emission[6]. CH_4 emissions from bog or swamp are highly variable and sensitive to soil temperature, while emissions from fen are additionally controlled by the dominating vegetation species[7]. Other factors that control the emissions are water table depth and pH. Complex interactions between temperature, other environmental variables and vegetation determine the CH_4 emissions from northern peatlands[8].

Biogenic volatile organic compounds (BVOC) emitted from wetlands are equivalent to only 1.5–3% of the carbon emitted as CH_4. Earlier studies have reported varying amounts of monoterpene emissions from wetlands[9–12]. Some studies have reported emissions below the detection limit[11] but emissions also up to 146 mg C $m^{-2} h^{-1}$ [13] have been observed. Monoterpenes were found to be the second most emitted group of BVOCs after isoprene when 82 compounds were measured from 2 to 10 cm depth in boreal peatland[13].

Atmospheric aerosol particles and their effects on cloud properties and lifetime are the most uncertain aspect of radiative forcing, and especially is so the effect of secondary aerosol particles on the forcing[2]. The atmospheric secondary aerosol formation, either from biogenic or anthropogenic origin, is responsible for producing about half of the cloud condensation nuclei (CCN)[14].

It has been shown that aerosol formation can be initiated by clustering of sulphuric acid and stabilizing bases[15–17], highly oxidized organic vapors[18] or iodine oxides[19]. Highly oxidized organic compounds (HOM), that have a very low volatility, have been shown to originate from the oxidation reaction of VOCs[20]. The formation of organic condensable material from the reaction between alpha-pinene and ozone has been known for long time[21], but more exact knowledge of the gas-phase reactions that produce the low volatile compounds has been developed recently[18,20,22,23]. Several VOCs have been shown to undergo fast auto-oxidation reaction that leads to the formation of low-volatile compounds[24,25]. After the first molecular-level discovery of extensive involvement of biogenic organic compounds in new particle formation[20] many more locations have been found[26], where the formation of HOMs is detected in the gas and particulate phase. Although it was suggested already 60 years ago that very low volatile organics are responsible on new particle formation and subsequent growth[27,28], the formation mechanism and chemical composition was unknown.

Here we introduce previously not recognized climatically relevant process in the atmosphere above wetlands. In addition to the large emissions of CH_4 wetlands emit also VOCs among others monoterpenes and sesquiterpenes. Even though the amounts are small, they are enough to initiate new particle formation and consecutively cloud formation and thereby, potentially, influencing the radiation balance of the planet. With accelerating global warming, large areas under permafrost will thaw and introduce new wetlands with carbon emissions[29,30], but also increase the number of newly formed particles. The particle formation aspect of wetlands is not well studied, only one
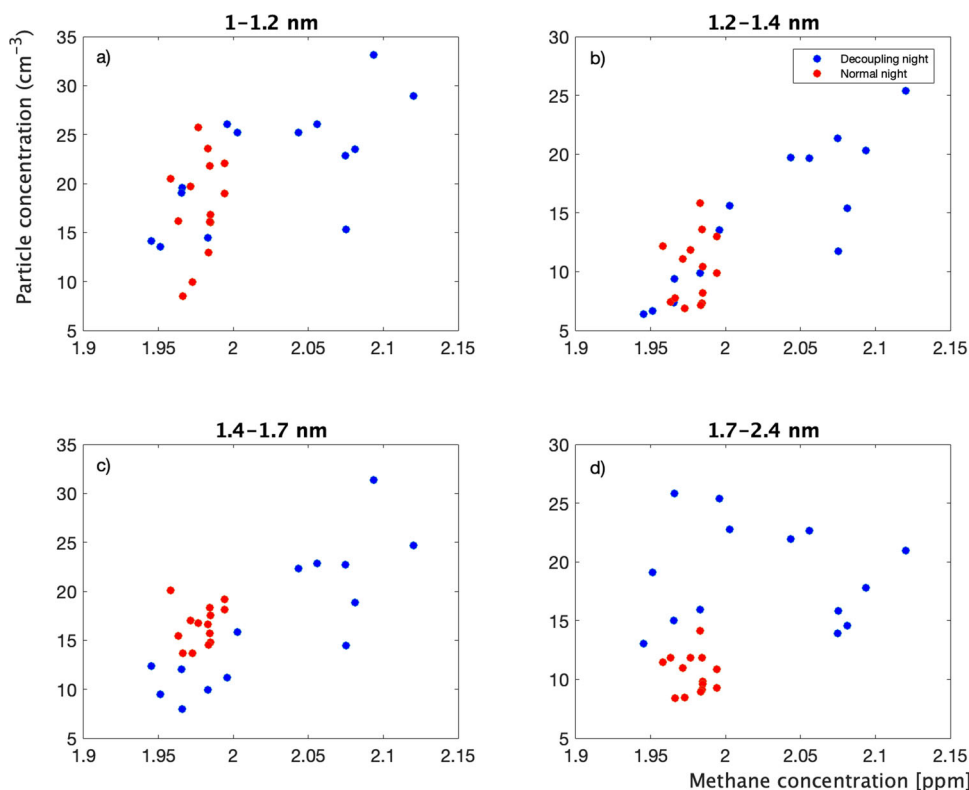
Fig. 1 Connection between methane and aerosol particle concentrations. Methane concentration (ppm) and 1–2.4 nm particle concentrations (cm^{-3}) during nights with decoupling (blue circles) and nights without decoupling (red circles). Median values of hourly means during night time (0:00–9:00, 18:00-00:00). Panel **a)** particle size 1–1.2 nm; **b)** particle size 1.2–1.4 nm; **c)** particle size 1.4–1.7 nm; **d)** particle size 1.7–2.4 nm.

publication was found where new particle formation was observed in the tundra ecosystem in a subarctic birch forest mixed with wetlands with minimal anthropogenic and boreal forest influence[1].

Results and discussion

Specific meteorological conditions characterized by clear skies and low wind speeds occur regularly throughout the year. At these conditions, a decoupled layer (or multiple superimposed layers) having a combined depth of about 0.5–4 m form over the wetland and the overlying inversion layers effectively isolate them from the rest of the nocturnal stable boundary layer (SI Figs S1 and S3). We observed the formation of this layer by monitoring turbulence and concentrations of CO_2 and CH_4 from different heights (1.5 m, 3 m) (see details in SI). By utilizing these measurements, we divided all nights into two groups; decoupling nights and normal nights (during our measurement period decoupling was detected on 40% of the nights). During the decoupling periods, all the emissions from the wetland are captured inside the stable boundary layer and nearly no mixing with the rest of the atmosphere occurs. Such "closed box" conditions made it possible to observe the potential of wetlands to produce new particles.

Due to surface emissions and subsequent chemical reactions, the concentration of 1.2–1.7 nm clusters/particles detected with the Particle Size Magnifier (PSM) increased at the same time with the CH_4 concentration (Fig. 1). Since this happens inside the isolated stable layer over the wetland, we conclude that CH_4 and the observed clusters originate from the same source, the wetland surface. Also, the nighttime formation rate of 1.5 nm atmospheric clusters increases significantly as a function of CH_4 concentration during the decoupling nights (Fig. 2). The formation rate of clusters increased by a factor of 4 as the decouple layering develops.

During daytime the aerosol concentrations in sub 3 nm size range (Fig. 3) and formation rate of 1.5 nm clusters/particles became significantly enhanced (Fig. 4) as a function of the CH_4
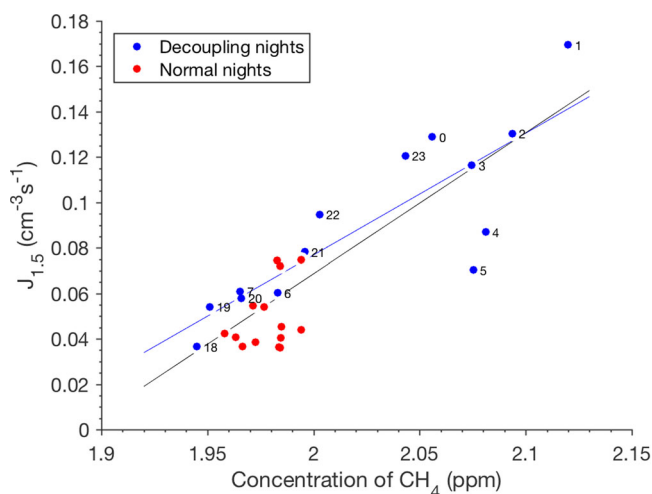

Fig. 2 Atmospheric aerosol particle formation rate and methane concentration. Connection between the 1.5 nm particle formation rate ($cm^{-3} s^{-1}$) and methane concentration (ppm). Diurnal median values of hourly values during the night time (18:00–9:00). Strong correlation does not imply that methane is responsible for enhanced formation rates, instead the emission of methane is a proxy of all emissions from wetland and the hour in consideration for decoupling nights marked in the figure. Blue fitting is only for decoupling nights ($J_{1.5} = 0.5544 * CH_4 - 1.033$, $R = 0.84$, $p < 0.05$) and black fitting for all nights ($J_{1.5} = 0.6026 * CH_4 - 1.1355$, $R = 0.85$, $p < 0.05$).

emissions (fluxes). This shows clearly that the CH_4 emissions and new particle formation (NPF) are connected to each other, but it does not mean the CH_4 is chemically involved in NPF. We can assume that the processes in wetlands, such as microbial activity in the peat, produces both CH_4 and terpenes[31], and therefore CH4 can be used as proxy for terpene production. However, based on current knowledge the CH_4 does not play a role in the chemistry behind NPF, rather the same process in wetland is producing both, CH4 and monoterpenes. In this study, we measured monoterpene emissions of 30 mg C m^{-2} h^{-1} (9.5 ng m^{-2} s^{-1}) (Supplementary Note 2, Fig. S4).

For the climatic relevance, the particles of sub-3 nm in size need to grow substantially larger. The material for the growth is provided by the formation of low volatile compounds. Here we observed correlation between concentrations of HOMs and sub-3 nm particles during the night time over the wetland (Fig. 5 and detailed scatterplots in Supplementary Note 3, Fig. S5–S7). The atmospheric mixing was minimal during the decoupling nights and this created conditions inside the isolated layer, where we observed strong increase in HOM concentrations that originated from the reaction between monoterpenes and O_3. These formed HOMs do not have a nitrogen atom in the molecule (denoted in the Fig. 5 as CHO monomer and dimer). In addition, also the HOMs from the sesquiterpene and O_3 reaction show clear elevated concentrations during decoupling nights and a strong correlation with sub-3 nm particles. On the contrary, the HOMs with nitrogen in the molecule (denoted as CHON and $CHON_2$) do not have significant increase during the decoupling nights and only the dimers of the HOM group with one nitrogen show a mild correlation with the sub-3 nm particle concentration (Fig. 5). The formation of nitrogen-containing HOMs only occurs when conditions are turbulent and a good mixing with the rest of the atmosphere exists. The same can be observed if looking only at one example day (20th–21th May, 2016 Figs. 6 and 7), where new particle formation together with an increase in the concentration of HOMs without nitrogen was observed. Nitrogen-containing HOMs and sulphuric acid concentration were decreasing during the particle formation event and it can be concluded that in this case, they were not participating in the particle formation and growth.

Figure 6 shows that the clusters formed in the decoupled layer above the wetlands contribute to the formation of large particles (instrument upper detection is 40 nm). In contrast with the clustering in the boreal forest during nighttime[32] (Supplementary note 4, Fig. S8) these cluster actually grow to sizes larger than 20 nm, contributing to the regional aerosol number budget, as in the morning hours these particles and remaining precursors are mixed upwards into the planetary boundary layer. Although we discovered the phenomena during the decoupling nights, peatlands emits monoterpenes all the time and contributes to total concentrations. In areas where wetlands are dominating, wetland-induced aerosol production can be a significant source of climatically relevant CCN. The whole process from clustering to 100 nm particles will take several hours (typically 10–40 h)[33].

In order to upscale the results, the spatial extent of the wetlands now and in the future climate scenarios must be taken into consideration. Current estimates for wetlands north of 30°N are 3.88–4.08 million km^2 [34–36]. In the boreal region (north of 50°N) wetlands make up more than 0.5 million km^2 (SI Fig. S9). This translates to 13 000 t C h^{-1} of monoterpene emissions from the boreal region, further, assuming 7% yield for conversion to HOMs[20,24,37] and all the HOM is condensing, about 900 t h^{-1} of organic carbon is condensing onto or forming new particles in the atmosphere over boreal wetlands. Considering the maximum boundary layer heights between about 1 and 2 km in boreal environments, such amounts of condensable organic material
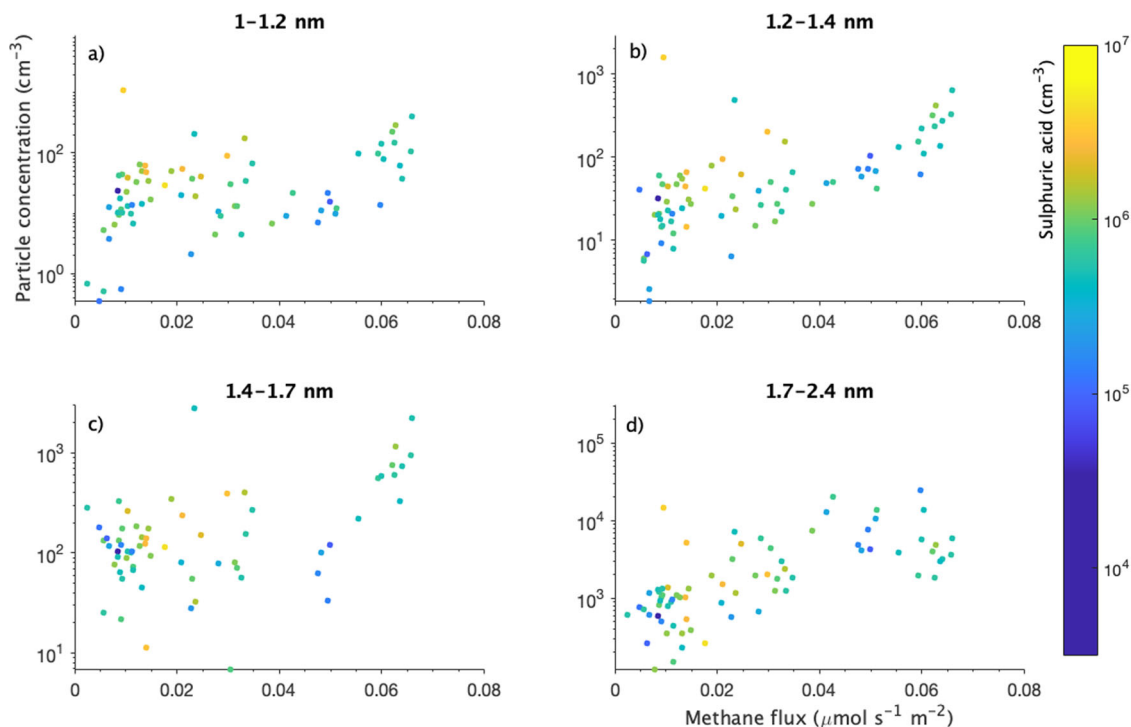
Fig. 3 Day time methane flux and atmospheric aerosol particle concentrations. Daily median values of methane flux (μmol s^{-1}m^{-2}) and cluster concentrations (cm^{-3}) during the light hours (09:00–15:00). Good correlation between the variables indicates the same source and not the causality. Color scale denotes the concentration of sulphuric acid, where no systematic features could be observed. This indicates a minor role of sulphuric acid in small particle formation over wetland. Panel **a**) particle size 1–1.2 nm; **b**) particle size 1.2–1.4 nm; **c**) particle size 1.4–1.7 nm; **d**) particle size 1.7–2.4 nm.
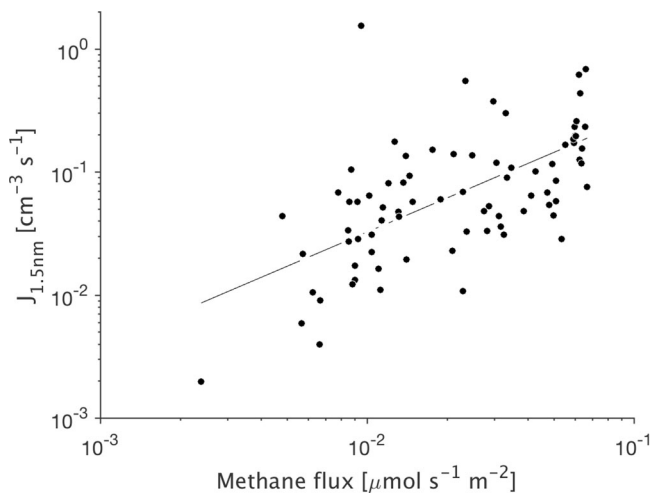

Fig. 4 Connection between methane flux and particle formation rate. Daytime (09:00–15:00) median values of methane flux (F_{CH_4}, μmol s^{-1}m^{-2}) and formation rate ($J_{1.5}$, cm^{-3} s^{-1}) of 1.5 nm particles measured with PSM. Correlation does not indicate direct causality, but instead an indication of the same origin for the both parameters. Depicted trendline follows an equation $J_{1.5} = 10^{(0.91 \cdot \log(F_{CH_4}) + 0.311)}$, $R = 0.63$, $p < 0.05$.

would be capable of producing 100-nm diameter particles at rates >1000 cm^{-3} h^{-1} over boreal wetlands. This is far more than the particle source strength needed for maintaining the observed populations of >100-nm particles in boreal environments[38], indicating that the rate-limiting step for the CCN formation from

wetland emissions is the particle formation rate rather than the growth of these particles to larger sizes.

As a summary, we have shown that wetlands emit terpenes and form atmospheric clusters and new aerosol particles. The freshly formed particles contribute to regional NPF events and, due to their further growth by condensable organic material formed from terpenes emitted by wetlands or nearby forested areas, to regional the CCN population. We further showed that the monoterpene emissions and resulting NPF occur concurrently with CH$_4$ emissions from wetlands. The wetland CH$_4$ emissions causes a warming effect on climate while, based on our results, the aerosol formation through wetland monoterpene emissions and oxidation leads to a cooling effect (Fig. 8). The overall magnitude of this balancing effect is difficult to estimate as it is constrained by wetland soil microbiology, boundary layer dynamics, atmospheric chemistry and cluster/aerosol dynamics. The interactions connect the warming (CH$_4$) and the cooling (aerosols, clouds) radiative forcing components together. Large-scale model studies have identified boreal forests as a major source of CCN to the atmosphere, with a potentially important cooling effect due to aerosol-cloud interactions[24,39]. This study demonstrates that, compared with boreal forests, boreal wetlands are even a stronger areal source of atmospheric clusters. Subsequential growth of these clusters is expected to lead to the formation of new CCN (CCN produced per m^2 of land) in the atmosphere, indicating that this effect needs to be considered when estimating the influences of wetlands on regional and global climate. The observed close connection between wetland CH$_4$ emissions and particle formation rate (Fig. 4) offers a means to incorporate the cooling effect due to wetland terpene emissions into any large-scale model capable of simulating atmospheric aerosol dynamics.
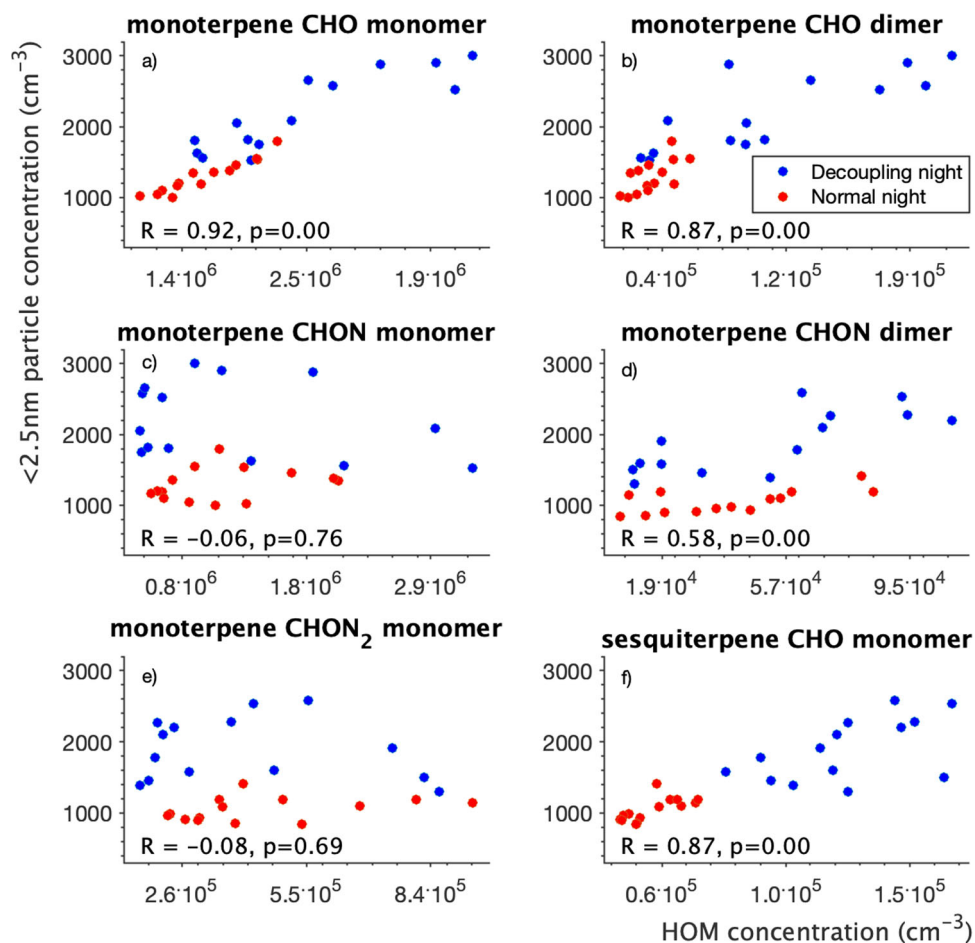
Fig. 5 Particle number concentration smaller than 2.5 nm and concentrations of different type of HOMs. Median values of hourly means during night hours (18:00–09:00). The HOMs are separated by the formation mechanism (see Table 1 in SI). HOMs formed from monoterpene and sesquiterpene in absence of NO_x are clearly responsible in particle formation, while HOMs that contain one or two nitrogen atoms are not well correlated with particles with the exception of CHON dimers. Correlation coefficient (R) and statistical significance (p) are calculated for all nights combined. Panel **a**) monoterpene oxidation products containing C, H, and O, 10 carbon-containing molecules; **b**) same as panel **a**) but 20 carbon molecules; **c**) monoterpene oxidation products containing C, H, O, and N. 10 carbon molecules; **d**) same as panel **c**) but 20 carbon molecules; **e**) monoterpene oxidation products containing C, H, O, and 2 N atoms, 10 carbon molecules; panel **f**) sesquiterpene oxidation products containing C, H, and O, 15 carbon molecules.

Methods

We deployed state-of-the-art instrumentation to Finnish wetland, Siikaneva (61°49′59.4″N 24°11′32.5″E, 162 m a.s.l.) where is located a class II ecosystem ICOS (European Integrated Carbon Observation System) station[40] and to SMEAR II station (Station for Measuring Ecosystem-Atmosphere Relations)[41], in Hyytiälä (61°50′47.1″N 24°17′43.2″E, 181 m a.s.l.) and investigated all the relevant components that are known to influence the new particle formation. The observations were performed on 10th May–15th June 2016. We monitored direct VOC and CH_4 emissions from wetland and the concentrations of oxidation products of VOCs, SO_2, and O_3. We monitored concentrations and chemical composition of atmospheric clusters, aerosols, and air ions from the smallest sizes (0.5 nm) up to 40 nm approaching sizes which can be activated to CCN. As a reference, we utilized SMEAR II station in Hyytiälä, located 5 km east of these measurements. The SMEAR II station is monitoring over 1200 variables, including also the ones measured in the Siikaneva wetland.

The Hyytiälä site is a relatively homogeneous Scots pine stand surrounded by evergreen coniferous forests[41], while the Siikaneva site is located in a pristine boreal fen. Peat started to accumulate in Siikaneva after the latest ice age about 9000 years ago and peat depth at the measurement site is approximately 4 meters[42,43]. Siikaneva fen is characterized by relatively flat topography with a number of vegetation communities and some surface patterning featuring drier hummocks and wetter lawns.

The measurement site consisted of a small hut containing all the instrumentation, which was equipped with sampling inlets at heights of approximately 1.5 m and 3 m. The CI-APi-TOF and APi-TOF, NAIS, PSM, O_3 measurements were conducted with the inlet at 1.5 m, while all the meteorological, CH_4, CO_2, and VOC data were obtained at 3 m.

Data sets from the SMEAR II station at Hyytiälä can be obtained from the AVAA smartSMEAR website (https://avaa.tdata.fi/web/smart)[44]. A detailed

description of the SMEAR II station at Hyytiälä can be found elsewhere[41,45]. Siikaneva station is part of ICOS (European Integrated Carbon Observation System) network that includes two classes of Ecosystem stations, referred to as Class 1 (complete) and Class 2 (basic) stations. They differ in costs of construction, operation, and maintenance due to the reduced number of variables measured at the Class 2 stations. Siikaneva station is classified as the class 2 ecology site.

Air temperature and relative humidity (RH) were measured with Rotronic HC2 sensor (Rotronic AG, Switzerland) at 2-meter height in Siikaneva. The air temperature was measured at 2 min and RH one minute time resolution. Photosynthetically active radiation (PAR) was measured once in a minute by a Li-Cor Li-190SZ quantum sensor (LI-COR, Inc., USA). Wind speed and direction were measured with Metek USA-1/Gill HS 50 anemometer at 3 meters height. The averaging period for all auxiliary measurements was 30 minutes.

VOC concentrations were measured with a proton transfer time-of-flight mass spectrometer (PTR-TOF, Ionicon) which consists of a proton transfer reaction ion source (PTR) and a TOF-MS[46]. The PTR instrument is described in detail in literature[47,48] and only short description is given here. The PTR consists of a H_3O+ ion source (hollow cathode discharge in water vapor) and a drift tube where protonated water is mixed with the sample and protons are transferred to the VOC species according to Eq. 1:

$$H_3O^+ + VOC \rightarrow VOCH^+ + H_2O \qquad (1)$$
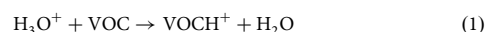
This charging mechanism works for VOCs with higher proton affinity than that of water, most atmospheric VOC fulfill this requirement[47].

The ionized $VOCH^+$ are then passed to the TOF and the mass is determined with an accuracy of 20ppt and resolving power of 3000Th/Th. The VOC is identified using the accurate mass and the prior made calibration. The concentrations of VOCs can be computed from the calibration as the ratio of sample to reagent ion
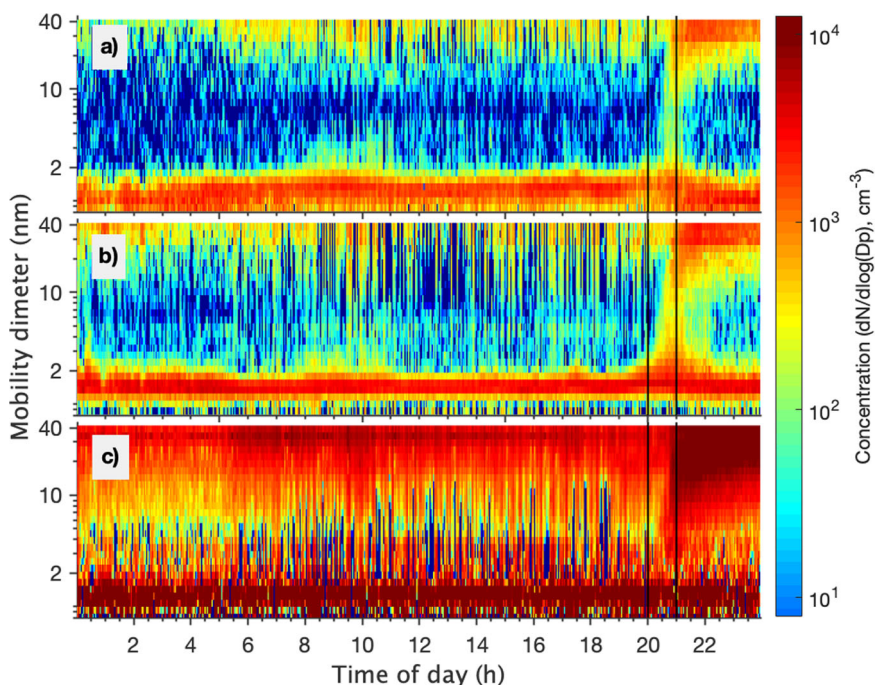
Fig. 6 Nighttime new particle formation and subsequent growth. Measured in Siikaneva 20.5.2016 with NAIS. Panel **a**) negative ions, panel **b**) positive and panel **c**) for neutral particles. Start of the event and the maximum growth period marked with black lines that correspond to the lines in Fig. 3c.

using equation Eq. 2:

$$[VOC] = [VOC^+]/([H_3O^+] \cdot kt) \qquad (2)$$

where $[H_3O^+]$ is the concentration of H_3O^+ in the absence of reacting neutrals, k is the reaction coefficient of the proton transfer reaction and t is the average time the ions spend in the reaction region[47]. Product kt is obtained from calibration.

Terpene and isoprene emissions are depended on temperature and light[49]. Accordingly, an increase in both concentrations is observed when approaching summer, indicating an increase in biogenic emissions (Supplementary note 6 and 7. Fig. S10-S12).

The chemical composition of air ions was measured with atmospheric pressure interface (APi) time of flight mass spectrometer[50] (APi-TOF, Tofwerk AG). The sample was driven to the instrument through 10 mm electropolished stainless steel tube with a flow rate of 6lpm. The sample was further introduced to APi through a critical orifice with a sample flow of 0.8 l min^{-1}, ions are transported into the TOF to determine their mass to charge ratio(m/Q). The ion beam is focused by two guiding quadrupoles and an ion lens assembly, in three separate differentially pumped chambers, leading into the TOF. The instrument has resolving power of >3000 Th/Th and mass accuracy <20ppm.

Second APi-TOF equipped with chemical ionization (CI) inlet was used to measure the concentration of highly oxidized organic molecules and sulphuric acid. The design of the CI-inlet is similar to one used earlier[51,52]. The sample was drawn though a ¾" electropolished stainless-steel tube with a flow rate of 10 lpm. Nitrate ions are created by exposing clean air containing nitric acid to a soft x-ray radiation. This sheath flow is then introduced in an ion reaction tube concentric to the sample flow. Nitrate ions in the sheath flow are directed into the sample flow by means of an electric field. The interaction time between ions and sample gas is approximately 200 ms.

The signal of highly oxidized organic compounds (HOMs) is distributed over multiple mass peaks. Example of spectrum is shown in supplementary note 7. Marker peaks were selected to represent each HOM group (Table 1). Concentrations of HOMs were calculated by assuming collision limited charging and the same calibration coefficient ($5 \cdot 10^{10}$) as for sulphuric acid according Eq. 3

$$C_{HOM} = \zeta \cdot \frac{\sum\limits_{m=1}^{n} I_m}{\sum\limits_{c=1}^{3} I_c}, \qquad (3)$$

where, ζ - calibration coefficient, I_m – signal intensity of HOM marker, I_c – signal intensity of charger ion, n – number of marker compounds of corresponding HOM group.

Calibration for sulphuric acid was performed prior the campaign in the laboratory by oxidation of SO_2 with OH to produce the sulphuric acid[53]. The hydroxyl radical is produced by UV photolysis of water vapor. The final H_2SO_4 concentration is calculated by a numerical model at the outlet of the calibration source. Comparison of this modelled concentration and the signals measured by CI-APi-TOF yields a calibration factor.

Comparison of Hyytiälä and Siikaneva sulphuric acid concentrations and diurnal patterns are shown in supplementary note 9, Fig. S17 and S18.

Atmospheric ions and total particles were measured with a Neutral cluster and Air Ion Spectrometer[54] (NAIS), an instrument for measuring mobility and size distribution. The range for electrical mobility for NAIS is 3.2-0.0013 cm^2 V^{-1} s^{-1} corresponding to a mobility diameter range of 0.8–42 nm. In total particle mode, the size distribution starts from 2 nm since the charger ions are indistinguishable at smaller particle size ranges[55,56].

For measurements of sub-3 nm particles, a Particle Size Magnifier (PSM) in series with a Condensation Particle Counter (CPC) was deployed. This setup enables the detection of single particles without charging the particles[57]. PSM uses diethylene glycol for activating and growing the particles before entering the CPC. This enables the detection of particles as small as ~1 nm in mobility diameter[57].

Growth Rates (GR) were determined using the 50% appearance time method[58,59]. This method uses particle size distributions measured by NAIS or DMPS instruments to determine the time when half the concentration maximum is reached in different size bins. The growth rate was obtained by following the evolution of the 50% appearance times as a function of the size distribution during clustering events.

Condensation Sinks (CS) for both measurement sites, Hyytiälä and Siikaneva, were calculated using the particle size distributions measured with the NAIS and DMPS instruments. Since there were measured at ambient conditions a para-meterization to correct for ambient hygroscopicity was used[60]. The CS describes the sink for condensing vapors arising from the available surface area of pre-existing aerosols and can be determined using the Eq. 4:

$$CS = 4\pi D \sum_{d_p} \beta_{m,d_p} d_p N_{d_p} \qquad (4)$$

where D is the diffusion coefficient of the condensing vapor, H2SO4 in our case, β_m, d_p refers to the transition regime correction[61], while N_{d_p} is the particle number concentration.

Condensation sink (CS) is usually calculated from DMPS data, since unlike NAIS (2 – 42 nm) it detects aerosol population up to 1000 nm. However, the DMPS system was not available at Siikaneva, and it was verified that calculating CS from NAIS data introduces larger systematic error than using CS calculated from Hyytiälä DMPS (Supplementary note 10, Fig. S19). The comparison of CS calculated from the NAIS shows a good linear correlation between the CSs determined for the two measurement sites (Supplementary note 10, Fig. S20). Error from using CS for Siikaneva calculated from Siikaneva NAIS compared to the Hyytiälä DMPS is larger and justifies the use of the CSs from Hyytiälä DMPS when determining formation rates at Siikaneva. Example clustering event measured simultaneously at two stations is depicted in supplementary note 11 in Fig. S21.

Formation rates (J_{dp}) were calculated for the Siikaneva measurement site based on the particle number size distribution, the coagulation sink and the determined
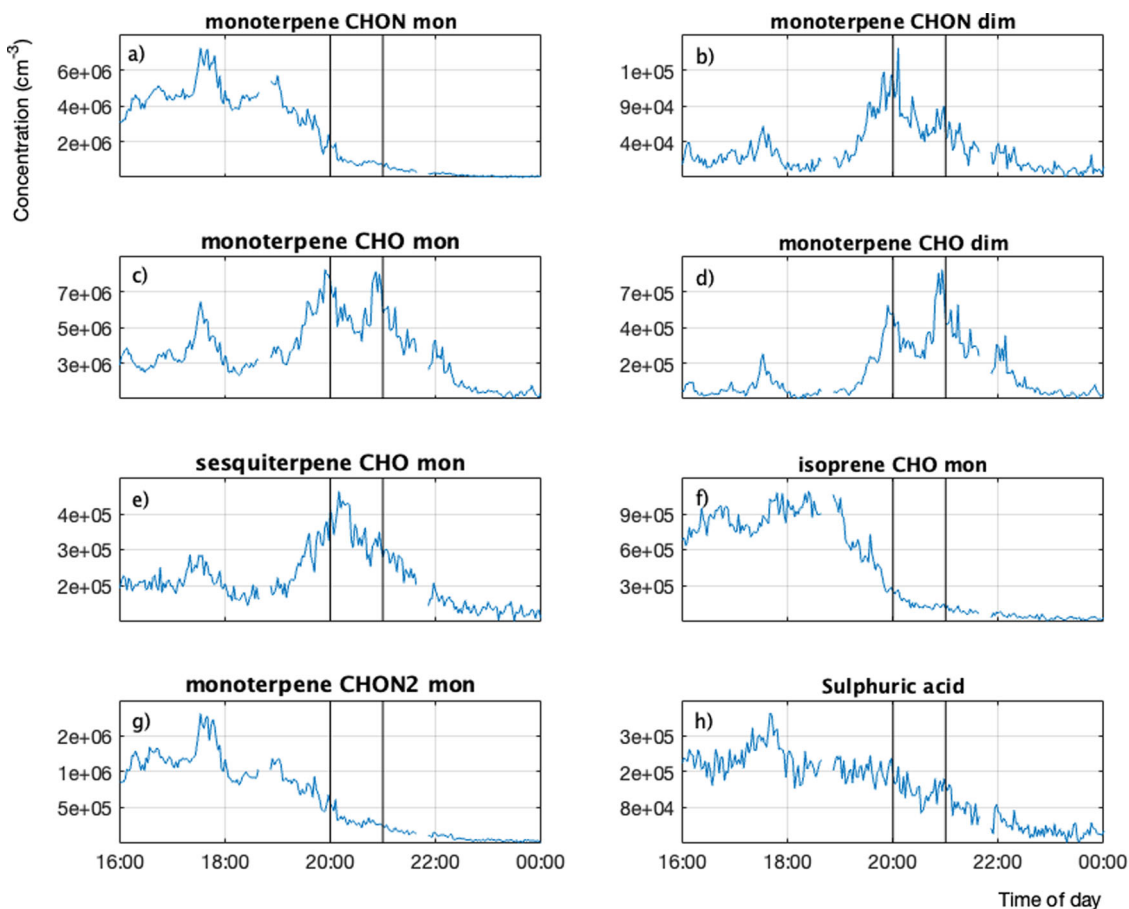
Fig. 7 HOM and sulphuric acid time series during NPF period. Mass spectrometric measurements with CI-APiTOF. Monoterpene CHO monomer and dimer HOMs have two peaks one at the start of the event and the other during the maximum growth period. Panel **a)** monoterpene oxidation products containing C, H, O, and N atoms, 10 carbon atoms containing molecules; panel **b)** same as panel a) but 20 carbon molecules; **c)** monoterpene oxidation products containing C, H, and O, 10 carbon atoms containing molecules; **d)** same as panel c) but 20 carbon molecules; **e)** sesquiterpene oxidation products containing C, H, and O, 15 carbon molecules; **f)** isoprene oxidation products containing C, H, and O, 5 carbon molecules; **g)** monoterpene oxidation products containing C, H, O, and 2 N atoms, 10 carbon atoms containing molecules; **h)** sulphuric acid.
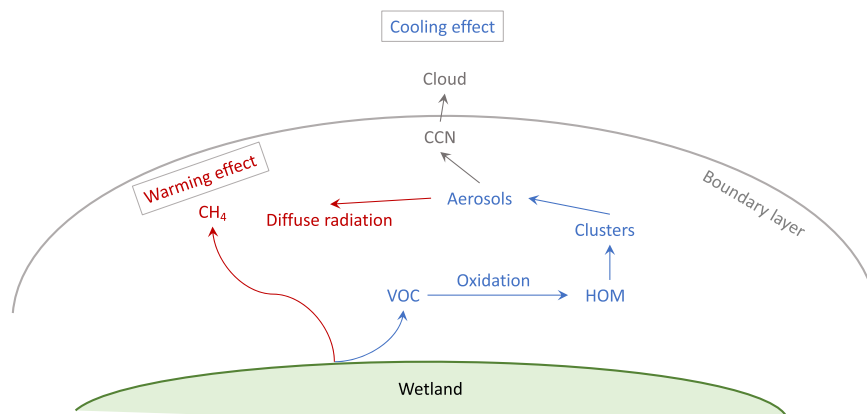

Fig. 8 Pathways of potential climatic effects of a wetland. Schematic figure connecting methane (CH_4) and volatile organic compounds (VOC, namely mono- and sesquiterpenes) in wetland and the potential (gray) climatic effect. The warming effect depicted in red and cooling one in blue.

GR[62] with Eq. 5

$$J_{d_p} = \frac{dN_{d_p}}{dt} + CoagS_{d_p} * N_{d_p} + \frac{GR}{\Delta d_p} N_{d_p} \qquad (5)$$

Where J_{dp} is the formation rate of the cluster with diameter d_p while $CoagS_{dp}$ is the coagulation sink arising from collisions with larger particles[63].

Greenhouse gas flux measurements, in this case carbon dioxide (CO_2) and methane (CH_4), were conducted with eddy covariance (EC) method at 3 meters height. CO_2 and water vapor (H_2O) flux measurements were done with high-frequency optical gas analyzer (LI- 7200, LI-COR Biosciences) and 3D sonic anemometer (USA-1, Metek GmbH; CSAT3 Campbell Scientific, Inc.). CH_4 flux was measured with CH_4 analyzer RMT-200 (Los Gatos Research Inc., Mountain View, California, USA) and 3D sonic anemometer (USA-1, Metek GmbH; CSAT3 Camp- bell Scientific, Inc.). CO_2 and CH_4 fluxes were measured every half an hour. Uncertain values of CO_2 and CH_4 fluxes were filtered out with friction velocity values less than 0.1 m s^{-1}. In Hyytiälä, net ecosystem exchange (NEE, CO_2 flux)

Table 1 Marker peaks for highly oxidized molecules.

Name	Elemental Composition (mass-to-charge ratio)	Abbreviation
Monoterpene CHO monomer	$C_{10}H_{14}O_7$ NO_3^- (308) $C_{10}H_{14}O_9$ NO_3^- (340) $C_{10}H_{14}O_{11}$ NO_3^- (372)	mt CHO mon
Monoterpene CHO dimer	$C_{19}H_{28}O_{11}$ NO_3^- & $C_{20}H_{32}O_{10}$ NO_3^- (494) $C_{20}H_{32}O_{11}$ NO_3^- & $C_{19}H_{28}O_{12}$ NO_3^- (510) $C_{20}H_{32}O_{13}$ NO_3^- & $C_{19}H_{28}O_{14}$ NO_3^- (542)	mt CHO dim
Monoterpene CHON monomer	$C_{10}H_{15}O_6N$ NO_3^- (307) $C_{10}H_{15}O_7N$ NO_3^- (323) $C_{10}H_{15}O_8N$ NO_3^- (339)	mt CHON mon
Monoterpene CHON dimer	$C_{20}H_{31}O_{11}N$ NO_3^- (523) $C_{20}H_{31}O_{13}N$ NO_3^- (555) $C_{20}H_{31}O_{15}N$ NO_3^- (587)	mt CHON dim
Sesquiterpene CHO monomer	$C_{15}H_{22}O_9$ NO_3^- (408) $C_{15}H_{22}O_{11}$ NO_3^- (440) $C_{15}H_{22}O_{13}$ NO_3^- (472)	sq CHO mon
Isoprene CHO monomer	$C_5H_9O_7$ NO_3^- (243) $C_5H_9O_8$ NO_3^- (259)	ip CHO mon
monoterpene CHON2 monomer	$C_{10}H_{16}O_9N_2$ NO_3^- (370) $C_{10}H_{16}O_{11}N_2$ NO_3^- (402)	mt CHON2 mon
monoterpene CHON2 dimer	$C_{20}H_{32}O_{10}N_2$ NO_3^- (522) $C_{20}H_{32}O_{12}N_2$ NO_3^- (554)	mt CHON2 dim
Reagent ions	NO_3^- (62), $HNO_3NO_3^-$ (125), $(HNO_3)_2NO_3^-$ (188)	-

was directly measured using Metek USA-1 anemometer and LI-COR LI-7000 gas analyzer.

Map product used to estimate the area of wetland was produced by European Space Agency Climate Change Initiative (ESA CCI) Land Cover project. The CCI-LC project delivers a consistent global land cover maps at 300 m spatial resolution on an annual basis from 1992 to 2015. The Coordinate Reference System (CRS) used for the global land cover databases is a geographic coordinate system (GCS) based on the World Geodetic System 84 (WGS84) reference ellipsoid.

The CCI-LC combined spectral data from 300 m and 1000 m resolution ENVISAT (MERIS) surface reflectance to classify land cover into 36 land cover types following the United Nations Land Cover Classification System (UNLCCS) legend[64,65]. The whole archive of MERIS data was first pre-processed for radiometric and geometric corrections, cloud screening, and atmospheric correction with aerosol retrieval. An automated classification process, combining supervised and unsupervised algorithms, was then applied to the full-time series to serve as a baseline to derive land cover maps that were representative of three 5-year periods[66]. The current updated product is provided in 1-year periods (ESA CCI[67]).

From CCI-LC maps we calculated the extent of wetlands located north from 30°N to be 1.2 million km^2. Equivalent values reported in the literature are 3.88–4.08 million km^2 [34–36]. The reliability of land cover estimations based on remote sensing data depends on the sampling, preprocessing and interpretation of the data. The observed discrepancy with earlier studies is therefore reasonable. The area of wetland in boreal region (north form 50°N) is 0.5 million km^2.

The highest density of wetland in north from 50°N is located in Siberia (31–180°E, $3.8\cdot10^5$ km^2), especially in areas of Khanty-Mansi and Yamalo-Nenets regions (60–90°E, $2.2\cdot10^5$ km^2), and in Scandinavia (5–31°E, $6.2\cdot10^4$ km^2) (SI Fig. 9).

References

1. Svenningsson, B. et al. Aerosol particle formation events and analysis of high growth rates observed above a subarctic wetland-forest mosaic. *Tellus B-Chem. Phys. Meteorol.* **60**, 353–364 (2008).
2. IPCC. *Climate Change 2013: The Physical Science Basis. Contribution of Working Group I to the Fifth Assessment Report of the Intergovern- mental Panel on Climate Change.* (Cambridge University Press, 2013).
3. Peltola, O. et al. *Monthly Gridded Data Product of Northern Wetland Methane Emissions Based on Upscaling Eddy Covariance Observations. Earth System Science Data Discussions* https://doi.org/10.5194/essd-2019-28 (2019).
4. Saunois, M. et al. The global methane budget 2000-2012. *Earth Sys. Sci. Data* **8**, 697–751 (2016).
5. Zhuang, Q. et al. CO_2 and CH_4 exchanges between land ecosystems and the atmosphere in northern high latitudes over the 21st century. *Geophys. Res. Lett.* **33**, 1–5 (2006).
6. Wuebbles, D. J. & Hayhoe, K. Atmospheric methane and global change. *Earth-Sci. Rev.* **57**, 177–210 (2002).
7. Turetsky, M. R. et al. A synthesis of methane emissions from 71 northern, temperate, and subtropical wetlands. *Global Change Biol.* **20**, 2183–2197 (2014).
8. Abdalla, M. et al. Emissions of methane from northern peatlands: a review of management impacts and implications for future management options. *Ecol. Evol.* **6**, 7080–7102 (2016).
9. Klinger, L. F., Zimmerman, P. R., Greenberg, P., Heidt, L. E. & Guenther, A. B. Carbon trace gas fluxes along a successional gradient in the Hudson Bay lowland. *J. Geophys. Res.* **99**, 1469–1494 (1994).
10. Rinnan, R., Rinnan, Å., Holopainen, T., Holopainen, J. K. & Pasanen, P. Emission of non-methane volatile organic compounds (VOCs) from boreal peatland microcosms — effects of ozone exposure. *Atmos. Environ.* **39**, 921–930 (2005).
11. Hellén, H., Hakola, H., Pystynen, K., Rinne, J. & Haapanala, S. C2-C10 hydrocarbon emissions from a boreal wetland and forest floor. *Biogeosciences* **3**, 167–174 (2006).
12. Janson, R., Serves, C. De & Romero, R. Emission of isoprene and carbonyl compounds from a boreal forest and wetland in Sweden. *Agric. Forest Meteorol.* **99**, 671–681 (1999).
13. Faubert, P. et al. Non-methane biogenic volatile organic compound emissions from boreal peatland microcosms under warming and water table drawdown. *Biogeochemistry* **106**, 503–516 (2011).
14. Merikanto, J., Napari, I., Vehkamaki, H., Anttila, T. & Kulmala, M. New parameterization of sulfuric acid-ammonia-water ternary nucleation rates at tropospheric conditions (vol 112, D15207, 2009). *J.Geophys. Res.-Atmos.* **114**, D09206 (2009).
15. Jokinen, T. et al. Ion-induced sulfuric acid–ammonia nucleation drives particle formation in coastal Antarctica. *Sci. Adv.* **4**, eaat9744 (2018).
16. Kirkby, J. et al. Role of sulphuric acid, ammonia and galactic cosmic rays in atmospheric aerosol nucleation. *Nature* **476**, 429–U77 (2011).
17. Almeida, J. et al. Molecular understanding of sulphuric acid-amine particle nucleation in the atmosphere. *Nature* **502**, 359–363 (2013).
18. Kirkby, J. et al. Ion-induced nucleation of pure biogenic particles. *Nature* **533**, 521–526 (2016).
19. Sipilä, M. et al. Molecular-scale evidence of aerosol particle formation via sequential addition of HIO3. *Nature* **537**, 532–534 (2016).
20. Ehn, M. et al. A large source of low-volatility secondary organic aerosol. *Nature* **506**, 476–9 (2014).
21. Christoffersen, T. S. et al. Cis-pinic acid, a possible precursor for organic aerosol formation from ozonolysis of α-pinene. *Atmospheric Environment* **32**, 1657–1661 (1998).
22. Bianchi, F. et al. New particle formation in the free troposphere: A question of chemistry and timing. *Science* **352**, 1109–1112 (2016).
23. Bianchi, F. et al. Highly Oxygenated Organic Molecules (HOM) from Gas-Phase Autoxidation Involving Peroxy Radicals: A Key Contributor to Atmospheric Aerosol. *Chemical Reviews* https://doi.org/10.1021/acs.chemrev.8b00395 (2019).
24. Jokinen, T. et al. Production of extremely low volatile organic compounds from biogenic emissions: Measured yields and atmospheric implications. *Proc. Natl. Acad. Sci. USA.* **112**, (2015).
25. Jokinen, T. et al. Production of highly oxidized organic compounds from ozonolysis of β-caryophyllene: Laboratory and field measurements. *Boreal Env.Res.* **21**, 262–273 (2016).
26. Bianchi, F. et al. Highly Oxygenated Organic Molecules (HOM) from Gas-Phase Autoxidation Involving Peroxy Radicals: A Key Contributor to Atmospheric Aerosol. *Chem. Rev.* https://doi.org/10.1021/acs.chemrev.8b00395 (2019).
27. Kulmala, M., Toivonen, A., Makela, J. M. & Laaksonen, A. Analysis of the growth of nucleation mode particles observed in Boreal forest. *Tellus Series B-Chemical and Physical Meteorology* **50**, 449–462 (1998).
28. Went, F. W. Blue hazes in the atmosphere. *Nature* **187**, 641–643 (1960).
29. Turetsky, M. R. et al. Permafrost collapse is accelerating carbon release. *Nature* **569**, 32–34 (2019).
30. Christensen, T. R. & Cox, P. Response of methane emission from arctic tundra to climatic change: results from a model simulation. *Tellus B.* **47**, 301–309 (1995).

31. Boronat, A. & Rodríguez-Concepción, M. Terpenoid Biosynthesis in Prokaryotes. *Adv. Biochem. Engi./Biotechnol.* .**14**, 83–18 (2015).

32. Junninen, H. et al. Observations on nocturnal growth of atmospheric clusters. *Tellus B-Chem. Phys. Meteorol.* **60**, 365–371 (2008).

33. Kerminen, V.-M. et al. Atmospheric new particle formation and growth: review of field observations. *Environ. Res. Lett.* **13**, 103003 (2018).

34. Wu, Y., Chan, E., Melton, J. R. & Verseghy, D. L. A map of global peatland distribution created using machine learning for use in terrestrial ecosystem and earth system models. *Geosci. Model Dev.* https://doi.org/10.5194/gmd-2017-152 (2017).

35. Yu, Z., Loisel, J., Brosseau, D. P., Beilman, D. W. & Hunt, S. J. Global peatland dynamics since the Last Glacial Maximum. *Geophys. Res. Lett.* **37**, 1–5 (2010).

36. Maltby, E. & Immirzi, P. Carbon dynamics in peatlands and other wetland soils. *Chemosphere* **27**, 999–1023 (1993).

37. Berndt, T. et al. Gas-Phase Ozonolysis of Selected Olefins: The Yield of Stabilized Criegee Intermediate and the Reactivity toward SO2. *J. Phys. Chem. Lett.* **3**, 2892–2896 (2012).

38. Maso, D. et al. Annual and interannual variation in boreal forest aerosol particle number and volume concentration and their connection to particle formation. *Tellus, Series B: Chemical and Physical Meteorology* **60**, 495–508 https://doi.org/10.1111/j.1600-0889.2008.00366.x (2008).

39. Sporre, M. K. et al. BVOC-aerosol-climate feedbacks investigated using NorESM. *Atmospheric Chemistry and Physics*, **19**, 4763–4782. https://doi.org/10.5194/acp-19-4763-2019 (2019).

40. Rinne, J. et al. Temporal Variation of Ecosystem Scale Methane Emission From a Boreal Fen in Relation to Temperature, Water Table Position, and Carbon Dioxide Fluxes. *Global Biogeochem. Cycles* **32**, 1087–1106 (2018).

41. Hari, P. & Kulmala, M. Station for measuring ecosystem-atmosphere relations (SMEAR II). *Boreal Environ. Res.* **10**, 315–322 (2005).

42. Rinne, J. et al. Annual cycle of methane emission from a boreal fen measured by the eddy covariance technique. *Tellus, Series B: Chemical and Physical Meteorology* **59**, 449–457 https://doi.org/10.1111/j.1600-0889.2007.00261.x (2007).

43. Mathijssen, P. J. H. et al. Reconstruction of Holocene carbon dynamics in a large boreal peatland complex, southern Finland. *Quat. Sci. Rev.* **142**, 1–15 (2016).

44. Junninen, H. et al. Smart-SMEAR: On-line data exploration and visualization tool for SMEAR stations. *Boreal Environ. Resarch.* **14**, 447–457 (2009).

45. Aalto, P. et al. Physical characterization of aerosol particles during nucleation events. *Tellus B-Chem. Phys. Meteorol.* **53**, 344–358 (2001).

46. Graus, M., Müller, M. & Hansel, A. High resolution PTR-TOF: Quantification and Formula Confirmation of VOC in Real Time. *J. Am. Society Mass Spectrom.* **21**, 1037–1044 (2010).

47. Hansel, A. et al. Proton transfer reaction mass spectrometry: on-line trace gas analysis at the ppb level. *Int. J. Mass Spectrom. Ion Processes* **149–150**, 609–619 (1995).

48. de Gouw, J & Warneke, C. Measurements of volatile organic compounds in the earth's atmosphere using proton-transfer-reaction mass spectrometry. *Mass Spectrom. Rev.* **26**, 223–257 (2007).

49. Lamb, B., Guenther, A., Gay, D. & Westberg, H. A. L. A national inventory of biogenic hydrocarbon emissions. *Atmos. Environ.* **21**, 1695–1705 (1987).

50. Junninen, H. et al. A high-resolution mass spectrometer to measure atmospheric ion composition. *Atmos. Meas. Tech.* **3**, 1039–1053 (2010).

51. Eisele, F. L. & Tanner, D. J. Measurement of the gas phase concentration of H_2SO_4 and methane sulfonic acid and estimates of H_2SO_4 production and loss in the atmosphere. *J. Geophys. Res.* **98**, 9001 (1993).

52. Jokinen, T. et al. Atmospheric sulphuric acid and neutral cluster measurements using CI-APi-TOF. *Atmos. Chem. Phys.* **12**, 4117–4125 (2012).

53. Kurten, A., Rondo, L., Ehrhart, S. & Curtius, J. Calibration of a Chemical Ionization Mass Spectrometer for the Measurement of Gaseous Sulfuric Acid. *J Phys. Chem. A* **116**, 6375–6386 (2012).

54. Mirme, S. & Mirme, A. The mathematical principles and design of the NAIS – a spectrometer for the measurement of cluster ion and Climate of the Past nanometer aerosol size distributions. *Atmos. Meas. Tech.* **6**, 1061–1071 (2013).

55. Asmi, E. et al. Results of the first air ion spectrometer calibration and intercomparison workshop. *Atmos. Chem. Phys.* **9**, 141–154 (2009).

56. Manninen, H. E., Mirme, S., Mirme, A., Petäjä, T. & Kulmala, M. How to reliably detect molecular clusters and nucleation mode particles with Neutral cluster and Air Ion Spectrometer (NAIS). *Atmos. Meas. Tech.* **9**, 3577–3605 (2016).

57. Vanhanen, J. et al. Particle Size Magnifier for Nano-CN Detection. *Aerosol Sci. Technol.* **45**, 533–542 (2011).

58. Dada, L. et al. Formation and growth of sub-3-nm aerosol particles in experimental chambers. *Nat. Protoc.* **15**, 1013–1040 (2020).

59. Kontkanen, J. et al. High concentrations of sub-3nm clusters and frequent new particle formation observed in the Po Valley, Italy, during the PEGASOS 2012 campaign. *Atmos. Chem. Phys.* **16**, 1919–1935 (2016).

60. Laakso, L. et al. Ion production rate in a boreal forest based on ion, particle and radiation measurements. *Atmos. Chem. Phys.* **4**, 1933–1943 (2004).

61. Fuchs, N. A. & Sutugin, A. G. *Highly dispersed aerosol*. (Pergamon, 1971).

62. Paasonen, P. et al. Connection between new particle formation and sulphuric acid at Hohenpeissenberg (Germany) including the influence of organic compounds. *Boreal Environ. Res.* **14**, 616–629 (2009).

63. Kulmala, M. et al. On the formation, growth and composition of nucleation mode particles ¨. *Tellus B-Chem. Phys. Meteorol.* **53**, 479–490 (2001).

64. Di Gregorio, A. & Jansen, L. J. M. *Land Cover Classification System (LCCS): Classification Concepts and User Manual.* (Food and Agriculture Organization of the United Nations, 2014).

65. Li, W. et al. Gross and net land cover changes in the main plant functional types derived from the annual ESA CCI land cover maps (1992-2015). *Earth Sys. Sci. Data* **10**, 219–234 (2018).

66. Poulter, B. et al. Plant functional type classification for earth system models: Results from the European Space Agency's Land Cover Climate Change Initiative. *Geosci. Model Dev.* **8**, 2315–2328 (2015).

67. Land Cover CCI Product Users Guide. (2017).

Acknowledgements

Author contributions

Planning and executed the measurement campaign A.L., B.F., Q.L., S.S. M.H.E, L.K., La.J., R.M., R.P., Le.J. Data processing and analysis D.L., B.M.S., K.J., N. S., A.D., G.O., A.P., L.H., T.K. Interpretation the results, commenting and writing the manuscript, S.M., E.M., W. D., Z.S., M.I., R.J., V.T., P.T., K.V.-M., K.M. Contributed to all stages of the study J.H.

Competing interests

The authors declare no competing interests.

Additional information

Supplementary information The online version contains supplementary material available at https://doi.org/10.1038/s43247-022-00406-9.

Correspondence and requests for materials should be addressed to Heikki Junninen or Markku Kulmala.

Peer review information *Communications Earth & Environment* thanks Nigel Roulet and the other, anonymous, reviewer(s) for their contribution to the peer review of this work. Primary Handling Editors: Jan Lenaerts, Joe Aslin. Peer reviewer reports are available.

Reprints and permission information is available at http://www.nature.com/reprints

Publisher's note Springer Nature remains neutral with regard to jurisdictional claims in published maps and institutional affiliations.